2301-9069 (e)
1829-8370 (p)

Kapal: Jurnal Ilmu Pengetahuan dan Teknologi Kelautan
(Kapal: Journal of Marine Science and Technology)

journal homepage : http://ejournal.undip.ac.id/index.php/kapal

Numerical Analysis on Added Resistance of a Crew Boat with Variation of Wave Period

Dita Adhelia Putri[1)], Muhammad Hafiz Nurwahyu Aliffrananda[2)], Sugeng Riyadi[3)], Sutiyo Sutiyo[4)], I Ketut Aria Pria Utama[1)]

[1)] Department of Naval Architecture, Institut Teknologi Sepuluh Nopember, Kampus ITS, Sukolilo, Surabaya, Indonesia, 60111, Indonesia
[2)] Department of Mechanical Engineering, the University of Melbourne, Melbourne, Australia, Australia
[3)] Orela Shipyard Plc, Gresik, Indonesia, Indonesia
[4)] Department of Naval Architecture, Universitas Hang Tuah Surabaya, Jalan Arief Rachman Hakim No. 150, Sukolilo, Surabaya, Indonesia, 60111, Indonesia

[*)] Corresponding Author: kutama@na.its.ac.id

Article Info

Keywords:
Crew Boat;
Added Resistance;
Added Power;
Wave Period;
CFD.

Article history:
Received: 29/08/2022
Last revised: 20/12/2022
Accepted: 27/12/2022
Available online: 27/12/2022
Published: 08/02/2023

DOI:
https://doi.org/10.14710/kapal.v20i1.48615

Abstract

Crew boat is a type of vessels used for the mobility of offshore workers and logistical supply needed for the offshore platform. Crew boat KCT-1901 is categorized as a planning boat with hard chine body. KCT-1901 requires an added power when it is sailing through a seaway. The reason behind this is because when a ship sails through a seaway, the ships experienced a heave and pitch motion resulted in added resistance and hence added power. The goal of the investigation is to estimate added resistance and added power of the crew boat using computational fluid dynamic (CFD) method and tested in calm water and in waves with several Froude numbers (Fr) and wave periods. A method developed by Savitsky is used for verification at high-speed mode. The largest total resistance using CFD in calm water is 38.98 kN and using Savitsky method is 39.00 kN obtained at Fr 0.72. Both are in good agreement and the discrepancy is less than 0.1%. Comparative study was carried out against experimental test in a towing tank. The drag forces tested at Fr 0.12 and 0.24, between the two approaches, showed a discrepancy of about 4%. Further CFD test was conducted on wave pattern analysis, which demonstrated that as the Fr increases the becomes clearer and stronger and tests in waves condition at lower wave period showed that the transverse wave becomes more apparent. CFD simulation showed the increase of added resistance as well as added power about 76% in waves compared to calm water condition. Therefore, overall can be said that the CFD simulation showed such a good agreement with empirical Savitsky method and experimental tank test.

Copyright © 2023 KAPAL: Jurnal Ilmu Pengetahuan dan Teknologi Kelautan. This is an open access article under the CC BY-SA license (https://creativecommons.org/licenses/by-sa/4.0/).

1. Introduction

1.1. Background

Crew boat is a type of vessel which is used to transport offshore workers and supply logistics required for offshore platforms. The boat is a type of planning hull craft which relies heavily on speed mode to satisfy energy efficiency [1]. Despite the issue of decarbonization, the demand and construction of crew boat tend to increase in the last 10 years. Among others, KCT-1901 is one of the offshore crew boats developed by Orela Shipyard to support oil drilling activities at Makassar Street (off-coast East Kalimantan Province) with a distance of approximately 100 miles from the coastline. The KCT-1901 boat has 17.8 m length and operated at high speed mode [2], the ability of ship to maintain its operational speed at sea is very crucial and become one of the main considerations for ship designers. Based on the above evident, resistance analysis of the KCT-1901 boat is carried out considering the operational performance of the ship which is operated at high speed. Furthermore, during the high-speed mode, wave-making resistance will increase thus causes additional resistance due to wave.

A comprehensive study is still needed to get useful data from the research related to added resistance due to waves. The additional resistance variation trend of Polar Research Vessel (PRV) is consistent with that of conventional ships, but PRV added resistance does not have a perfect quadratic relationship with wave amplitude [3].

Hydrodynamic effects have little influence on heave and pitch for a Froude number 0.142, but add resistance due to pure hydrodynamic effect and the total added resistance are affected considerably by wave height and scale ratio [4]. Waterline integral has been determined to contribute the most to the increased resistance, and in long waves, this happens at the waterline's forwardmost point [5]. According to a logarithmic derivative study of the EFD data, the additional resistance (AR) and propulsive efficiency (η) are respectively responsible for 70 vs. 30% AP for head waves and 55 vs. 38% AP for oblique waves. where, the experimental and CFD approaches are accurate enough to be useful for design [6].

The investigation is conducted numerically using computational fluid dynamics (CFD) approach to quantify the added wave resistance at various speeds. As a continuation of the previous work done [7], this study used a crew boat type as its research design vessel. The results of the CFD simulation are confirmed by using the empirical Savitsky technique and by conducting ship model tests at a towing tank. This is done after the findings have been verified in accordance with the rules of the ITTC. In spite of this, not all of the CFD data is validated experimentally due to the fact that there is not enough space remaining and the test is too costly. The findings of CFD simulations on additional resistance and additional power are particularly important as considerations for the industry to make through order to improve efficiency while operating crew boats in rough conditions.

1.2. Resistance of Ship

The term added resistance describes the phenomenon of energy loss caused by waves and wind due to movement of the ship hence ship's resistance will increase [8]. As the ship enters the open sea, which wave heights increase, the achieved speed will be less than the ship operating speed. Therefore, the boat must increase the power to maintain the service speed. Unfortunately, the fuel consumption and hence the emission will increase accordingly. In this case, the so-called added wave resistance is responsible for speed reduction and on delay in ship arrival at the destination port.

Although not new, research on added resistance has been a major concerned for ship designers for many years. Among others, better ship design together with optimization have been widely implemented to reduce the added resistance thus the fuel consumption and safety of ships at sea can be handled properly [9]. For practical purposes, experts in the past suggested the additional margin between 10% and 30%, depending on routes, to cover the effect of added resistance [10,11]. As the wave resistance is dependent on Froude scale [8], the variable of speeds can be obtained from the value of Froude number (Fr) using the following formula, as seen in Equation 1:

$$Fr = \frac{V}{\sqrt{gL}} \tag{1}$$

The total ship resistance (R_T) and wave resistance (R_W) can be calculated using Equations 2 and 3, respectively:

$$R_T = \frac{1}{2} C_T \rho S V^2 \tag{2}$$

$$R_W = \frac{1}{2} C_W \rho S V^2 \tag{3}$$

Where, R_T is total ship resistance (N), R_W is wave resistance (N), C_T is total ship resistance coefficient, C_W is wave resistance coefficient, ρ is density of water (998 kg/m^3), v is speed of the ship (m/s), S is wetted surface area (m^2)

Whilst, the calculation of wave resistance can be done using the Havelock theory [12], see Equation 4:

$$R_{AW} = -\frac{k}{2}(F_A z_A sin\epsilon_{zF} + M_A \theta_A sin\epsilon_{\theta M}) \tag{4}$$

Effective power (P_E) can be calculated using Equation 3 [11], which can also be used to calculate the added wave resistance when ship is operated in waves.

$$P_E = R_T \mathrm{V} \tag{5}$$

In the case of planning hull (such as crew boat), the total hydrodynamic resistance of ship can be estimated using Equation (6) [13]:

$$D = \Delta tan(\tau) + \frac{\varphi V^2 C_F \Delta B^2}{2cos(\beta)cos(\tau)} \tag{6}$$

2. Material and Methods

Principle particulars of the vessel are shown in Table 1 and the designs are shown in Figure 1.

Table 1. Principle particulars of the ship

Parameter	Value	Unit
Length of Over All (LOA)	17.8	m

Length between perpendiculars (LBP)	16.83	m
Breadth (B)	4.5	m
Height (H)	2.2	m
Draught (T)	0.95	m
Displacement (Δ)	36.43	ton

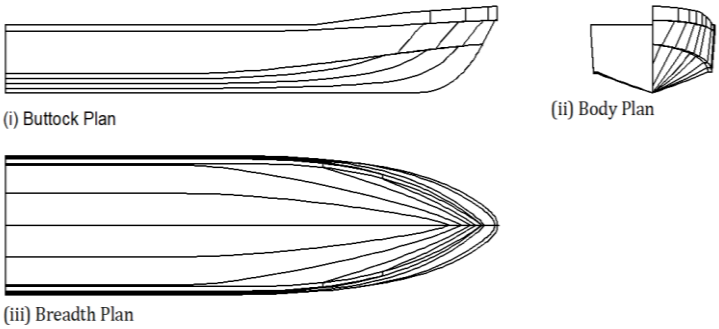

Figure 1. Design of KCT-1901 [7]

3-D model is later created, using Maxsurf Design Modeller, based on the lines plan data. The results will not be certainly precise and a maximum error of 2% is allowed [14]. The comparison of ship data and 3-D model is shown in Table 2 and the geometry of 3-D model is shown in Figure 2.

Table 2. Comparison of ship data with 3D model

Parameter	Unit	Ship Data	3D Model	Discrepancy (%)
LOA	m	17.8	17.8	0%
LBP	m	16.83	16.81	0.13%
B	m	4.5	4.5	0%
H	m	2.2	2.2	0%
T	m	0.95	0.95	0%
Displacement	ton	36.43	36.46	0.08%

Figure 2. 3-D Model of KCT-1901

2.1. Numerical Simulation

The power requirements of the ship's main engine operated at a certain speed in calm waters and in waves can be estimated using the forces obtained from numerical simulations. Numerical simulation was carried out using two-phase of fluids, i.e., air and sea water (multi fluid/free surface simulation), in accordance with real conditions when the ship is operated at sea. The numerical simulation is carried out using continuity equation, Reynolds-Averaged Navier-Stokes Equation (RANSE), and turbulence k-w SST-Menter model to solve the turbulence phenomena. The equations for those three are shown in Equations 7 to 9. Furthermore, the CFD setup and variation of numerical test using CFD are provided in Tables 3 and 4, respectively.

$$\frac{\partial U_i}{\partial x_i} = 0 \tag{7}$$

Where: ρ is fluid density, t is time, U_j is the flow velocity vector field.

$$\frac{\partial U_i}{\partial t} + U_j \frac{\partial U_j}{\partial x_j} = \frac{\partial p}{\partial x_i} + \frac{\partial}{\partial x_j}\left[Re_{eff}^{-1}\left(\frac{\partial U_i}{\partial x_j} + \frac{\partial U_j}{\partial x_i}\right)\right] + S_i \tag{8}$$

where U_i = (u, v, w) represented Reynolds average velocity components; x_i = (x, y, z) signified the independent coordinate direction; the term Si denoted the mean strain-rate tensor for a body force, the piezometric pressure p, and the Re_{eff} were effective Reynolds numbers.

The Menter′s SST model combines the advantages of the *k-ω* model to achieve an optimal model formulation for a wide range of applications. For this, a blending function *F1* is introduced which is equal to one near the solid surface and equal to zero for the flow domain away from the wall. It activates the *k-ω* wall region and the *k-ε* model for residual flow. By this approach, the attractive near-wall performance of the *k-ω* model can be used for the free stream sensitivity.

$$\frac{\gamma}{v_t}P - \beta\rho\omega^2 + \frac{\partial}{\partial x_j}\left[(\mu + \sigma_\omega\mu_t)\frac{\partial\omega}{\partial x_j}\right] + 2(1-F_1)2\rho_{\omega 2}\frac{1}{\omega}\frac{\partial k}{\partial x_j}\frac{\partial\omega}{\partial x_j} - \left(\frac{\partial(\rho\omega)}{\partial t} + \frac{\partial(\rho u_j\omega)}{\partial x_j}\right) = 0 \quad (9)$$

Table 3. CFD Setup

Flow model (time configuration)	Unsteady
Fluid model	Multi fluid (air and water)
Turbulence model	Turbulence k–ω (SST-Menter)
Body motion	2 DOF (heave and pitch)
Dynamic mesh	Mesh deformation method
Output	Drag force
	Translation (heave)
	Rotation (pitch)
	Flow illustration

Table 4. Variation of numerical test CFD

Full Scale Parameter					
Draft [m]	Period [s]	Amplitude [m]	Wavelength [m]	Heading Angle	Fr
0.95	2.58	0.25	10.37	180°	0.12
	4.12		26.55		0.24
	5.67		50.20		0.36
	7.22		81.31		0.48
					0.60
					0.72

2.2. CFD Verification

Numeca Fine/Marine® states the boundary conditions are presented in Figure 3. reducing computing complexity and demand can be accomplished by representing only half of the hull (the starboard side) [15]. One of the domain faces of the model was aligned along the centerline of the domain, in order to mimic the other half of the model. For the purpose of drawing, it should be mentioned that on certain figures, the mirror reflection of the ship and domain is shown on the port side.

The computational domain was illustrated in Figure 3. However, to the ship's symmetry, exactly half of the ship is represented. This was located 2L upstream from the vessel, and 6L downstream from the vessel. The side wall measures 3L on either side of the vessel. Bottom wall is 3L below the vessel, while top wall is 3L above the vessel (L is the length between the perpendiculars, LPP).

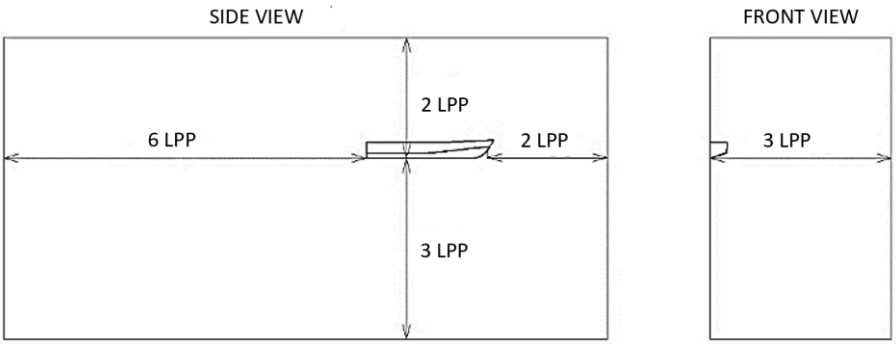

Figure 3. Computational domain for KCT-1901

An illustration of making grids on KCT-1901 is shown Figure 4. It can be seen that more and denser grids are placed closed to the body surface. The mesh consisting of rectangular elements is constructed on the hull surface, and the boundary layer is then refined with hexahedral elements by gradually expanding the surface mesh. According to

ITTC, hexahedral components are inflated to fill the area all around the boat in order to detail the interaction of air and water on the hull of the crew boat, together with the generation of waves [16]. It is intended to be able to capture the flow in area behind and around the object. Furthermore, grid independence study is carried out to fulfil the so-called computationally efficient and the results are shown in Table 5. It is apparent that grids of approximately 3.83 million elements is sufficient for used for the numerical simulation of KCT-1901. Grid independence study test was carried out at the Froude number 0.72 with the drag coefficient (C_T) value parameter. The 3.83 million elements demonstrated a discrepancy of 0.97% in total drag when compared with the 1.8 million elements. The result satisfies the criteria of maximum differences of less than 2% according to Anderson [17]. the simulation carried out is an unsteady simulation, a definition is needed regarding time. The definition of the time step (t) is 0.009 s, which was adjusted to the velocity of the fluid using Equation 10.

$$\Delta t = 0.005 \frac{L_{PP}}{v_{ref}} \quad (10)$$

Where, Δt is time step (s), L_{PP} is length perpendicular of crew boat (m), vref is velocity of crew boat (m/s)

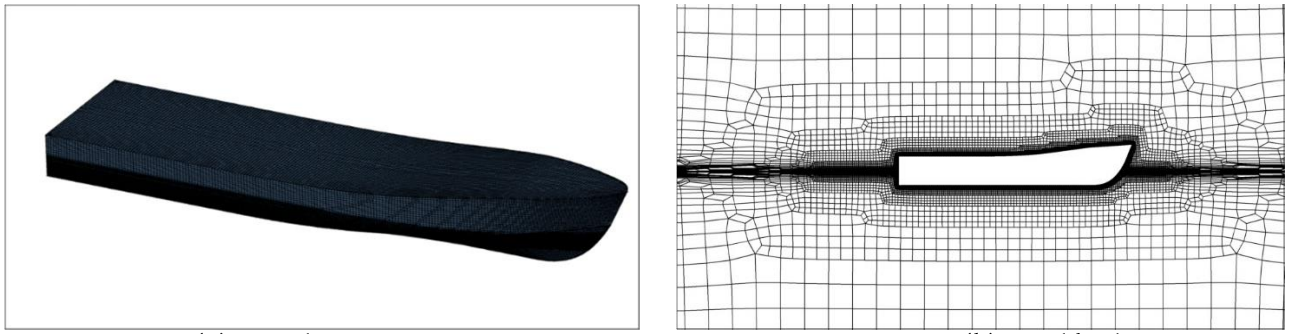

(a) 3-D view (b) 2-D side view

Figure 4. KCT-1901 grid shape used in CFD simulation

Table 5. Grid independence study KCT-1901

Total Number of Cells	Drag Force [kN]	Drag Coefficient (C_T)	Deviation
462,271	30.743	9.28×10^{-3}	-
931,892	35.628	10.76×10^{-3}	13.71 %
1,804,625	38.542	11.64×10^{-3}	7.56 %
3,831,253	38.919	11.75×10^{-3}	0.97 %
7,942,142	38.978	11.77×10^{-3}	0.15 %

A layer with a high aspect ratio is inserted into the anisotropic cells subdivision so as to get a high enough resolution to the flow. For cells close to the wall, it is necessary to take into account the variations in the wall y^+, according to Equation 11:

$$y^+ = \frac{\rho u_\tau y_{wall}}{\mu} \quad (11)$$

In the simulation, the value of y^+ is given by C-Wizard and the length between the perpendiculars (LBP) uses the Lref reference line. Number of y^+mentioned in ITTC (2014), thus by the C-Wizard recommendation $30 < y^+ < 80$ in which the strong agreement between model testing and CFD calculations for total ship resistance in calm water results in a high degree of trust [18].

2.3. Validation

Validation in the present study was carried out by comparing the results of CFD simulation against experimental test results using a towing tank. The results are accepted if the discrepancy is less than 5% [19]. Table 6 presents a comparison of the results of total resistance between the towing test and CFD simulation. The average discrepancy or difference between CFD and the experiment was 4.37%.

Table 6. Comparison of C_T of KCT-1901

Fr	Full Scale Wave Period [s]	Drag Coefficient (C_T)		
		CFD	Experiment	Difference
0.12	7.22	35.09×10^{-3}	33.63×10^{-3}	4.14%
	5.67	57.23×10^{-3}	54.81×10^{-3}	4.22%
	4.12	72.85×10^{-3}	69.64×10^{-3}	4.40%
0.24	7.22	18.88×10^{-3}	16.07×10^{-3}	4.29%

5.67	26.27×10^{-3}	25.08×10^{-3}	4.55%
4.12	32.62×10^{-3}	31.12×10^{-3}	4.60%

2.4 Heave and Pitch Motion

The motion equation uses two coordinate systems. One is the body-fixed coordinate system (Gξζ). At the center of gravity (CG). The ζ -axis is parallel to the base line and positive. The -axis is parallel to the base line and positive downward. The second system (OXZ) is a stationary straight coordinate system that moves with the boat's forward speed. Figure 5 depicts the boat's forces and moments in motion. The hydrodynamic force (F_{HD}), buoyancy force (F_B), and associated moments (M_{HD} and M_B) are all included.

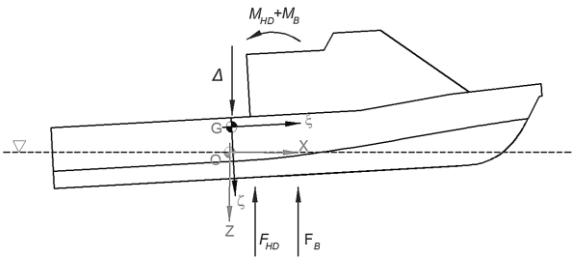

Figure 5. Coordinate system and force acting in Planning Hull

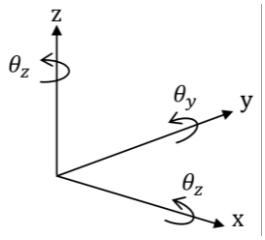

Figure 6. Coordinate system six degrees of freedom of body

The calculation of ship resistance involves the interaction between hull and fluid, which is commonly known as FSI (Fluid-Structure Interaction) [20]. These are obtained by calculating the vessel's equations of motion and rotation under the influence of the surrounding fluids and gravity. The number of directions a body may move and rotate is termed its degrees of freedom (DOF). Coordinate system that illustrates a rigid body's six degrees of freedom, as shown at Figure 6. These include translation and rotation along three axes in the x, y, and z parameters. In this study, crew boat resistance analysis was carried out in trim conditions which were influenced by heave and pitch only. Newton's second law describes the translational motion of the center of gravity for a rigid body, as Equation 12.

$$F = m\frac{dv}{dt} \tag{12}$$

Where m is the mass, v is velocity and F is the sum of forces acting on the body. Then, the rotation of the body, expressed in body coordinates, is described by Euler′ s Equation 13.

$$\tau = M\frac{d\omega}{dt} + \omega\ x\ (M.\omega) \tag{13}$$

Where ω is the angular velocity of the body and τ is the resultant torque acting on the body. Furthermore, M is a tensor of the moments of inertia and it is expanded into Equation 14.

$$M = \begin{bmatrix} M_{xx} & M_{xy} & M_{xz} \\ M_{yx} & M_{yy} & M_{yz} \\ M_{zx} & M_{zy} & M_{zz} \end{bmatrix} \tag{14}$$

3. Results and Discussion

3.1. Drag Force

Predictions related to the magnitude of the ship's drag force are carried out using two methods: (i) empirical calculations using Savitsky method for calm water conditions and (ii) numerical method based on CFD for calm water conditions and regular waves. The results are shown in Table 7. The CFD calculation verification is carried out by comparing the Savitsky calm water method. This verification shows a very small difference in value, which is around 0.07%, so that the CFD calculations were carried out in good condition. The resistance value in wavy waters shows a significant increase, as shown in Table 7. The biggest resistance occurs in the (T) 2.58s period with a resistance value of 65.603 kN, and the smallest resistance is 41.35 kN, which occurs in the (T) wave 7.22 s. This increase in resistance occurs due to the striking between the bow and the water waves. This interaction provides additional resistance for the ship. With a lot of wave intensity in the 2.58 s wave period, the addition of ship resistance becomes more significant.

Table 7. Drag force prediction of KCT-1901

Fr	Drag Force [kN]					
	Savitsky Calm Water	CFD Calm Water	CFD Regular Wave, T = 2.58s	CFD Regular Wave, T = 4.12s	CFD Regular Wave, T = 5.67s	CFD Regular Wave, T = 7.22s
0.12	-	1.001	8.602	6.700	5.263	3.227
0.24	-	4.498	15.143	12.002	9.666	6.946
0.36	-	12.361	25.241	21.499	18.625	14.648
0.48	-	25.674	41.424	36.455	32.945	27.995
0.60	33.60	33.572	53.872	47.095	42.361	35.920
0.72	39.00	38.978	65.603	56.684	49.418	41.353

3.2. Added Resistance

The total resistance of KCT-1901 is predicted in calm water and in waves using CFD technique. Added resistance is obtained from the difference between total resistance at calm water and in waves, see Table 8. The added resistance calculation can be seen in Table 8.

Table 8. Prediction of the amount of added resistance

Fr	Added Resistance [kN]			
	T = 2.58 s	T = 4.12 s	T = 5.67 s	T = 7.22 s
0.12	7.601	5.698	4.262	2.226
0.24	10.466	7.305	4.969	2.248
0.36	12.881	9.139	6.265	2.288
0.48	15.750	10.781	7.271	2.321
0.60	20.300	13.523	8.789	2.348
0.72	26.626	17.707	10.441	2.376

It is apparent from Table 8 that added resistance increase as the speeds (or Froude numbers) increase and this is attributed to the formation of wave-making which increases as the speed enlarges. Furthermore, at the same Froude number, added resistance decreases as the wave period increases. There is an additional resistance of an average of 76% when compared to the calculation of the resistance in calm water. the research results obtained are relevant to those carried out by Chen, et. al [21] that there was an additional resistance due to waves of up to 34% in displacement vessels and up to 40% [22]. The difference in added resistance in the current and past studies is due to the different types of ships. however, all studies that have been carried out show a significant addition of resistance in wavy water conditions.

3.3. Added Power

Calculation of added power is carried out based on the results of added resistance using Equation 4 but R_T (total resistance) is replaced with added resistance. Results of the calculations are presented in Table 9.

Table 9. Power Effective

Fr	Power Effective (HP)					
	Savitsky Calm Water	CFD Calm Water	CFD Regular Wave T = 2.58 s	CFD Regular Wave T = 4.12 s	CFD Regular Wave T = 5.67 s	CFD Regular Wave T = 7.22 s
0.12	-	1.545	13.276	10.340	8.123	4.980
0.24	-	14.500	46.743	37.047	29.836	21.440
0.36	-	57.2294	116.867	99.541	86.235	67.821
0.48	-	158.494	255.726	225.050	203.382	172.822
0.60	289.280	259.063	415.709	363.413	326.882	277.185
0.72	361.140	360.932	607.485	524.896	457.611	382.931

It can be seen in Table 8 that the values of power effective (P_E) has the same trend as the resistance values because power effective is a function of the ship's speed and resistance. Power effective increases with the increases of speed and decreases of wave period. The lowest P_E is achieved in calm water condition when Fr 0.12 and wave period 7.22 s, whilst the highest P_E is obtained in waves condition at Fr 0.72 and wave period 2.58 s. The results of P_E calculation can be found in Table 9. The lowest P_E (3.435 HP) occurs at Fr 0.12 and wave period 7.22 s, whilst the highest P_E (246.553 HP) occurs at Froude number 0.72 and wave period 2.58 s. The increase of crew boat power has an inverse proportional relationship with the wave period as shown in Table 10. The CFD method allows for water in wave conditions with variation from 2.58 s to 7.22 s, showing an average power increase of 76%. The most power is

required at the 2.85 s wave period. This power requirement has gone up by an average of 126.0%. The average increase in power needs during the 7.22 s wave period was the least, at 35%.

Table 10. Added Power

Fr	Added Power [HP]			
	CFD Regular Wave, T = 2.58 s	CFD Regular Wave, T = 4.12 s	CFD Regular Wave, T = 5.67 s	CFD Regular Wave, T = 7.22 s
0.12	11.731	8.795	6.578	3.435
0.24	32.243	22.547	15.336	6.940
0.36	59.637	42.312	29.005	10.592
0.48	97.231	66.556	44.888	14.327
0.60	156.646	104.349	67.819	18.121
0.72	246.553	163.964	96.679	21.999

3.4. Wave Pattern Analysis

When the crew boat moves on the water, the surface of water will respond to produce wave pattern and its contour dependent on the speed of the boat. Around the body surface and bottom of KCT-1901, the wave pattern will be formed that resembles the actual contour when operated on water. Figure 7 illustrates the contour of wave patter when operated in calm water after 30s. It is obvious that as the speed (and hence Froude number) increases, the contour of wave pattern becomes stronger and more visible. Furthermore, Figure 8 shows the shape of wave pattern when operated in regular wave with wave height 0.5m. The transverse wave is formed in waves, which is not in calm water condition. It is apparent that the formation of transverse wave becomes clearer and stronger as the speed increases.

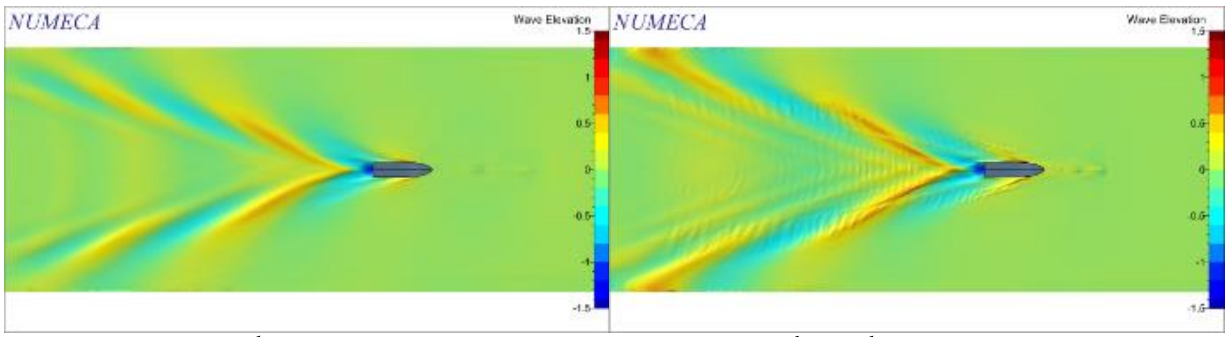

a. *Calm water* Fr = 0.60 b. *Calm water* Fr = 0.72

Figure 7. Contour of wave pattern in calm water

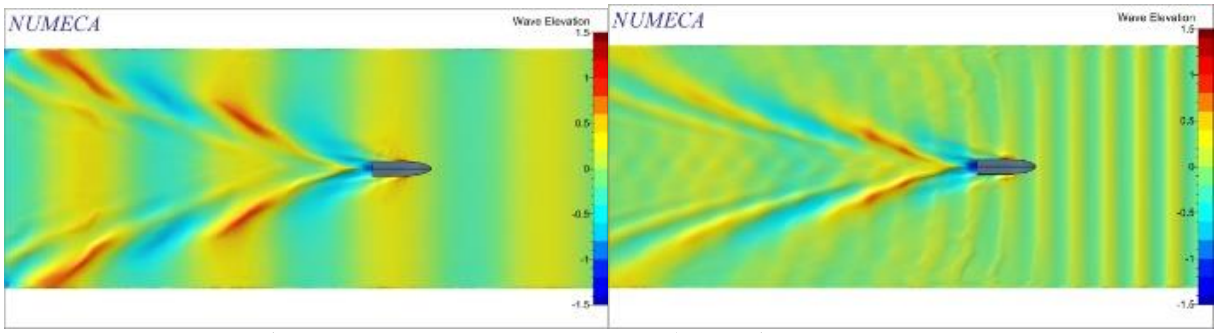

a. *Regular wave* Fr 0.72 T = 5.67s b. *Regular wave* Fr 0.72 T =2.58s

Figure 8. Contour of wave pattern in regular wave.

3.5. The Effect of Heave and Pitch

Two degrees of freedom of KCT-1901 was activated, namely heave and pitch motions. This was carried out to seek the effect of wave speed and period on heave and pitch motions of the boat since the test was done at head sea condition (180º). Illustrations of the ship motion are shown in Figures 9 and 10. It is apparent that spray is formed in the forward area and wave breaking in the stern area when the boat is tested in waves condition.

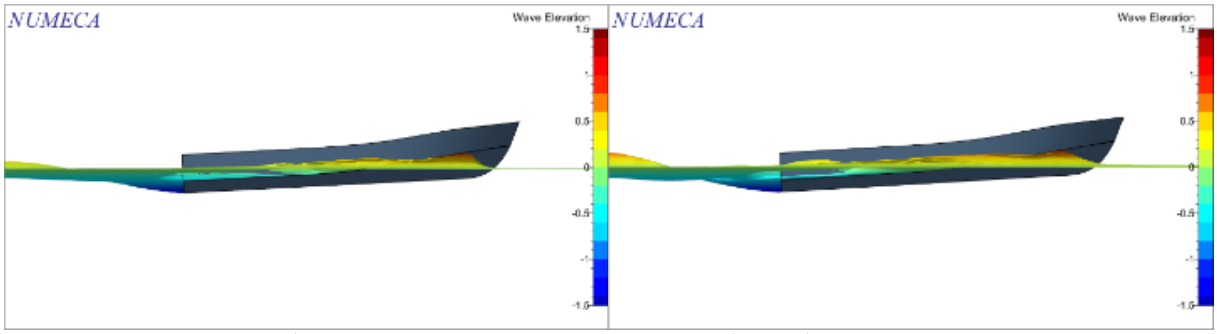

a. *Calm water* Fr = 0.60 b. *Calm water* Fr = 0.72

Figure 9. Heave and pitch motions in calm water

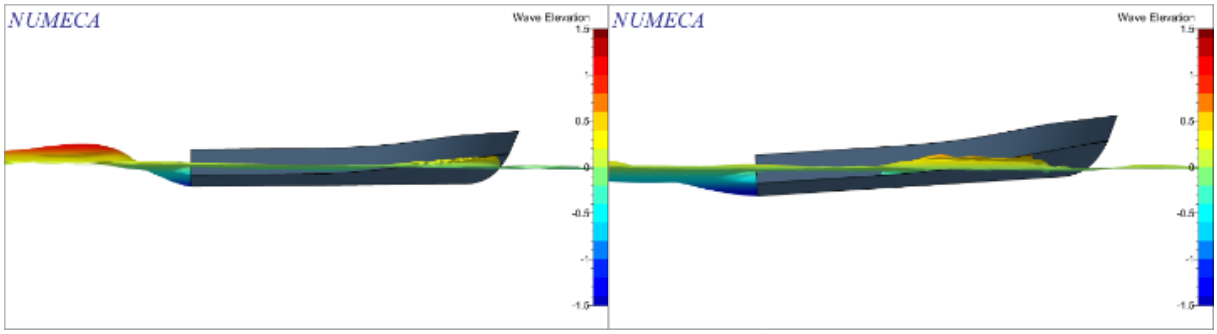

a. Fr = 0.48 T = 7.22 s b. Fr = 0.48 T = 2.58 s

Figure 10. Heave and pitch motions in regular wave

3.6. Wetted Surface Area

Water volume fraction (in term of CFD) or wetted surface area (WSA) (in term of naval architecture) is crew boat body areas which directly contact with water. WSA has direct effect on the magnitude of resistance related to the amount of added resistance [9]. WSA increases as the Froude number increases as shown in Table 10 for calm water condition. The similarity is also shown in Table 11 when tested in regular wave. However, this is different when compared on different wave period. It is clear in Table 11 that as the wave period increases, the WSA value decreases. This caused by motion of the ship due to waves hitting the ship's hull.

Table 8. The relationship of WSA to the speed of KCT-1901 in calm water

Calm Water	
Speed [Fr]	WSA [m^2]
0.12	37.53
0.24	37.65
0.36	37.94
0.48	38.33
0.60	38.73
0.72	39.01

Table 9. The relationship of WSA to the speed of KCT-1901 in regular wave

WSA on Regular Wave [m^2]						
Wave Period [s]	Fr 0.12	Fr 0.24	Fr 0.36	Fr 0.48	Fr 0.60	Fr 0.72
7.22	37.96	38.33	38.64	38.98	39.30	39.67
5.67	38.14	38.51	38.89	39.25	39.58	40.08
4.12	38.37	38.74	39.13	39.52	39.87	40.44
2.58	38.67	39.03	39.47	39.85	40.23	40.82

To provide an illustration related to WSA that occurred on the crew boat KCT-1901, an illustration is given in the form of a bottom view of the ship which appears in Figure 11 and Figure 12. It is obvious that as the speed increases, the formation of wave contour becomes clearer and stronger (see Figure 12). This does not occur at calm water condition (see Figure 11).

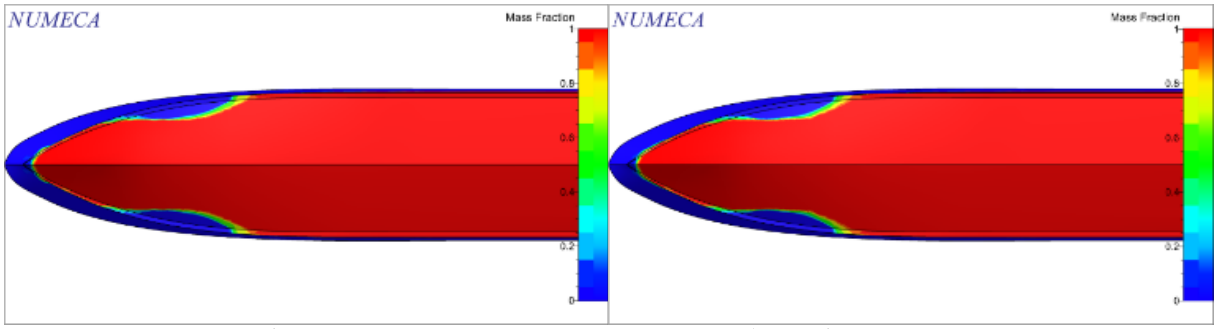

a. *Calm water* Fr = 0.60 b. *Calm water* Fr = 0.72

Figure 11. Bottom view of water volume fraction KCT-1901 in calm water

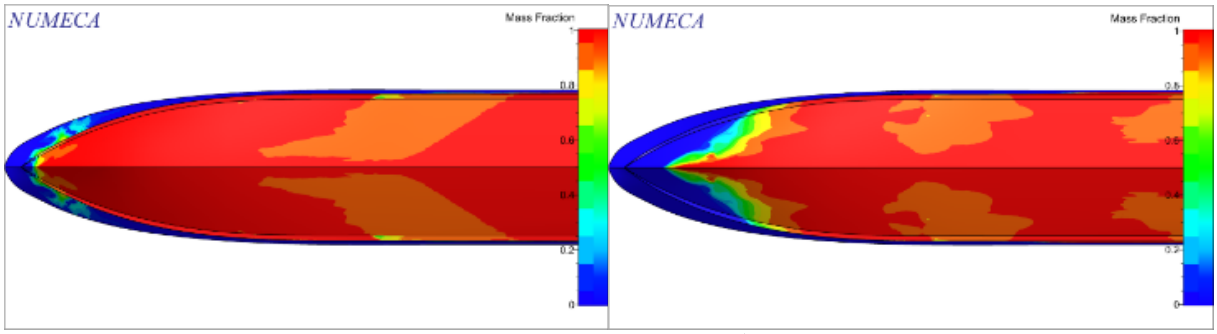

a. Fr = 0.72 T = 4.12 s b. Fr = 0.72 T = 2.58 s

Figure 12. Bottom view of water volume fraction KCT-1901 in regular wave

4. Conclusion

Numerical simulation using CFD method has been carried out on a crew boat to predict its total resistance both in calm water and in waves. The method is validated using empirical Savitsky method and experimental test using a towing tank. Overall, the three approaches demonstrated such a very good agreement. CFD simulation and Savitsky method showed a discrepancy of less than 0.1% when tested at the highest Froude number (Fr = 0.72). The difference between CFD and experimental test (at Froude numbers 0.12 and 0.24) is about 4% which is also satisfactory based on common recommendation of less than 5%. Wave pattern analysis showed that more apparent and stronger wave pattern were formed at higher Froude numbers indicating the formation of spray in the front area and wave breaking in the stern area.

Finally, added resistance and power effective which were calculated solely using CFD method, tested in calm water and in waves conditions, showed that the added power and power effective increases and the speed (or Froude number) increases. The results of the CFD simulation that has been carried out offer an estimate of the increase in resistance (added resistance), as well as an average effective power of 76% in comparison to calm water conditions. However, the added resistance and power effective decreases as the wave period increases. The addition of resistance gives the impact of increasing power requirements. This research is very useful for providing input to the industry in operating crew boats in wavy water conditions in the form of follow-up related to calculations for efficient use of fuel

Acknowledgements

The work is part of Newton Fund research between the Institut Teknologi Sepuluh Nopember (ITS) and the University College London (UCL) entitled "Ensuring the safety of crews and fishers onboard ships in the era of COVID-19 and beyond." Therefore, the authors wished to thank Prof. Giles Thomas from UCL for any suggestion given.

References

[1] D. Endro W, "High Speed Ship Total Resistance Calculation (An Empirical Study)," *Kapal: Jurnal Ilmu Pengetahuan dan Teknologi Kelautan*, vol. 11, no. 1, pp. 13. – 20, 2014, doi: doi.org/10.14710/kpl.v11i1.6338.

[2] D. Matulja, M. Sportelli, C. Guedes Soares, and J. Prpic-Orsic, "Estimation of Added Resistance of a Ship in Regular Waves," *Brodogradnja*, vol. 62, pp. 259–264, Sep. 2011.

[3] C. Chen, Y. Liu, Y. He, Z. Chen, and G. Zheng, "Numerical analysis of added resistance in head waves on a Polar Research Vessel and conventional ships," *Ocean Engineering*, vol. 233, p. 108888, 2021, doi: https://doi.org/10.1016/j.oceaneng.2021.108888.

[4] J. Yao, Y. Su, X. Song, Z. Liu, X. Cheng, and C. Zhan, "RANS Analysis of the Motions and Added Resistance for KVLCC2 in Head Regular Waves," *Applied Ocean Research*, vol. 105, p. 102398, 2020, doi: https://doi.org/10.1016/j.apor.2020.102398.

[5] X. Song, X. Zhang, and R. F. Beck, "Numerical study on added resistance of ships based on time-domain desingularized-Rankine panel method," *Ocean Engineering*, vol. 248, p. 110713, 2022, doi: https://doi.org/10.1016/j.oceaneng.2022.110713.

[6] Y. Sanada., D. Kim., H. S. Hosseini., F. Stern., M. A. Hossain., P.C. Wu., Y. Toda., J. Otzen., C. Simosen., M. A. Maksoud., M. Scharf., G. Griporopoulos, "Assessment of EFD and CFD capability for KRISO Container Ship added power in head and oblique waves," *Ocean Engineering*, vol. 243, p. 110224, 2022, doi: https://doi.org/10.1016/j.oceaneng.2021.110224.
[7] S. Riyadi, W. D. Aryawan, and I. K. A. P. Utama, "Experimental and Computational Fluid Dynamics Investigations into the Effect of Loading Condition on Resistance of Hard-Chine Semi Planning Crew Boat," *International Journal Technology.*, vol. 13, no. 3, pp. 518–532, 2022, doi: 10.14716/IJTECH.V13I3.4597.
[8] A. F. Molland, S. R. Turnock, and D. A. Hudson, *Ship Resistance and Propulsion*. Cambridge University Press, 2017.
[9] A. F. Molland, S. R. Turnock, D. A. Hudson, and I. K. A. P. Utama, "Reducing Ship Emissions: A Review of Potential Practical Improvements in the Propulsive Efficiency of Future Ships," *International Journal of Maritime Engineering*, vol. 156, no. A2, p. 175, Jun. 2014, doi: 10.3940/rina.ijme.2014.a2.289.
[10] S. A. Harvald, *Resistance and Propulsion of Ships*. Wiley, 1983.
[11] E. V Lewis, *Principles of NavalArchitecture Second Revision Volume II • Resistance , Propulsion and Vibration*, vol. II. 1988.
[12] R. Bhattacharyya, *Dynamics of marine vehicles*. New York, USA.: John Wiley & Sons Inc, 1978.
[13] D. Savitsky, "Hydrodynamic design of planing hulls," *Marine Technology*, vol. Vol. 1(1), pp. 71–95, 1964.
[14] T. Lamb (Editor), *Ship Design and Construction*. Society of Naval Architects and Marine Engineers, 2003.
[15] ITTC, "Recommended Procedures and Guidelines-Practical Guidelines for Ship Resistance CFD No. 7.5–03 –02–04," in *27th International Conference Towing Tank*, 2014, pp. 31 August–5 September. Denmark.
[16] ITTC, "Uncertainty analysis in CFD Verification and validation methodology and procedures," in *28th International Towing Tank Conference, Wuxi, China, September 17-22*, 2017.
[17] J. D. Anderson, *Computational Fluid Dynamics: The Basics with Applications*. New York, USA. pp. 526-532: McGraw-Hill, 1995.
[18] Marintek, "Marine Customer Cases | NUMECA International," 2021. [Online]. Available: https://www.numeca.com/marine-case/id/129. [Accessed: 29-Jul-2021].
[19] I. K. A. P. Utama, "Investigation of the viscous resistance components of catamaran forms (Ph.D Dissertation)," University of Southampton, UK., 1999.
[20] M. Diez., E. J. Lee., A. M. Powers., A. M. Fullerton., R. R. Lewis., E. L. Harrison., F. Stern., "FSI and MDO for Weight Reduction of a Grillage Panel of a Fast Deep-V Planing Hull Subject to Slamming in Waves," in *33rd Symposium on Naval Hydrodynamics*, 2020.
[21] C. Chen, Y. dong Liu, Y. ping He, Z. Chen, and G. yao Zheng, "Numerical analysis of added resistance in head waves on a Polar Research Vessel and conventional ships," *Ocean Engineering*, vol. 233, p. 108888, Aug. 2021, doi: 10.1016/J.OCEANENG.2021.108888.
[22] S. A. Hulsbergen, "Prediction of the added resistance in waves using CFD," Delft University of Technology, 2019.